Structures, Structural Dynamics, and Materials and Co-located Conferences
April 8-11, 2013, Boston, Massachusetts
54th AIAA/ASME/ASCE/AHS/ASC Structures, Structural Dynamics, and Materials Conference

SDM 2013 Student Papers Competition

A Rayleigh-Ritz Model for Dynamic Response and Buckling Analysis of Delaminated Composite Timoshenko Beams

Jared D. Hobeck[1] and Matthew B. Obenchain[2]
Department of Aerospace Engineering, University of Michigan, Ann Arbor, MI, 48108

This paper investigates the structural dynamic characteristics of laminate beams with various types of damage. More specifically, this work focuses on modeling delaminations of various sizes and locations within cantilevered laminate beams. Presented here is a Rayleigh-Ritz model which accounts for transverse and axial beam deformation as well as first-order shear deformation. Axial and bending stiffness properties of the beam are modeled using classical lamination theory. It is shown that the proposed Rayleigh-Ritz method greatly simplifies derivation, implementation, and computational cost of existing methods while still providing accurate results. Results show the effects of delamination size and location on the natural frequencies, mode shapes, and buckling loads of cantilever beams. Results from the analytical model are compared to those found using commercial finite element modeling software. Further comparisons will be made between the proposed model, and existing analytical and finite element models.

Nomenclature

A	=	cross sectional area
E	=	modulus of elasticity
EI	=	bending rigidity
h	=	height of beam or beam sublayer
I	=	area moment of inertia
N_x, N_y	=	normal force resultant in x and y direction respectively
N_{xy}	=	shear force resultant in xy plane
M_x, M_y	=	moment resultant about the y and x axis respectively
M_{xy}	=	shearing moment resultant
k	=	shear correction factor
k_S	=	distributed shear spring constant
k_N	=	distributed normal spring constant
P	=	applied axial load
T	=	kinetic energy
u,v,w	=	displacement in the x, y, and z directions respectively
W, Ψ ,U	=	shape functions for bending, shear, and axial deflections respectively
Π	=	potential energy
ν	=	Poisson's ratio
ρ	=	mass density
σ	=	stress from distributed normal spring
τ	=	stress from distributed shear spring
ψ	=	rotation of transverse normal
ω	=	angular frequency

[1] Ph.D. Candidate, Department of Aerospace Engineering , University of Michigan, 1320 Beal Avenue, Ann Arbor, MI, 48109, Mail Code 2140, AIAA Member
[2] Ph.D. Candidate, Department of Aerospace Engineering , University of Michigan, 1320 Beal Avenue, Ann Arbor, MI, 48109, Mail Code 2140, AIAA Member

I. Introduction

As composite structures are increasingly used in aerospace applications, understanding damage phenomena is correspondingly important. Delamination of composite lamina is one of the most common damage modes and can severely affect the performance capabilities of structures by reducing strength and stiffness. While quality control procedures have substantially decreased the presence of delamination flaws due to manufacturing processes, the introduction of damage in fielded systems remains a major concern. Dynamic analysis of composite structures can be used to both detect damage and characterize the effects of damage once it has been found.

Numerous studies in literature have considered the effects of delamination on the dynamic behavior of bonded homogeneous beams and composite beams. Della and Shu[1] presented a thorough review of these studies. The subset of studies most pertinent to this paper is categorized as the "region approach" in their review. They credit Ramkumar et al.[2] with the first model for vibration in delaminated composite beams, in which the beam was separated into three spanwise sections with a through-width delamination in the middle region. This model is known as a "free mode" model since the transverse displacments of the delaminated layers are not constrained. Mujumdar and Suryanarayan[3] introduced a "constrained mode" model that related the transverse displacements of the delaminated layers to one another and corrected for physically inadmissible mode shapes. Shen and Grady[4] later presented an analytical model using Timoshenko beam theory and performed experiements to validate their model. The parameters for these experiments have often been used as a baseline for comparison with other models[1] and will be used in this paper as well. Della and Shu[5] used a model combining seven Euler-Bernoulli beams to depict overlapping delaminations. Their work bounded the natural frequencies of the beam by using both a "free mode" model and a "constrained mode" model. Luo and Hanagud[6] and Qiao and Chen[7] developed models that use distributed springs between the delaminated regions, allowing models between the "free mode" and "constrained mode" case to be considered. These two models form the primary basis for this work and will be explained further in the paper.

The proposed approach described in this paper demonstrates how results similar to those found from these rigorous analytical models can be attained using the Rayleigh-Ritz method. The primary advantages of employing a Rayleigh-Ritz method to solve this problem are ease of implementation and minimal computational effort. Beginning with the potential and kinetic energy expressions for a simplified delaminated beam, this paper will show how one can directly construct mass and stiffness matrices and solve the vibration eigenvalue problem for natural frequencies and mode shapes. Another advantage of the approach shown in this study is that after the vibration eigenvalue problem is setup, it is then straightforward to solve for the buckling eigenvalue problem. The goal of this paper is to model delamination in symmetric composite beams using the proposed approach and then validate the method through comparison to other numerical and experimental data. The effect of delamination on natural frequencies, mode shapes, and buckling load is the primary area of interest. All results will be compared to those found with a pristine beam specimen to quantify the damage effects.

In general, this paper will focus on the behavior of a clamped-free beam constructed using a symmetric composite laminate. The overal beam dimensions are shown in Fig. 1 and listed in Table 1. The laminate is of cross-ply construction with a $[0/90/0/90]_S$ configuration as illustrated in Fig. 2. The material properties used throughout this paper correspond to a T300/934 graphite/epoxy lamina and are summarized in Table 1. As mentioned earlier, the dimensions and properties match those used in several previous studies in the literature[1], allowing for direct comparison to published results.

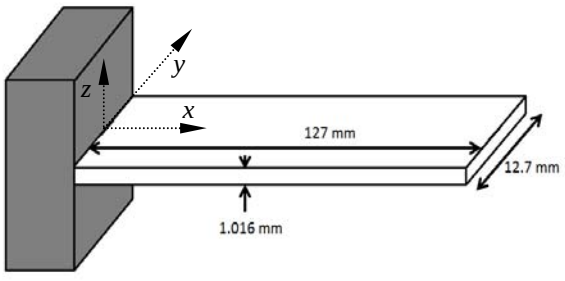

Figure 1. Dimensions of beam specimen

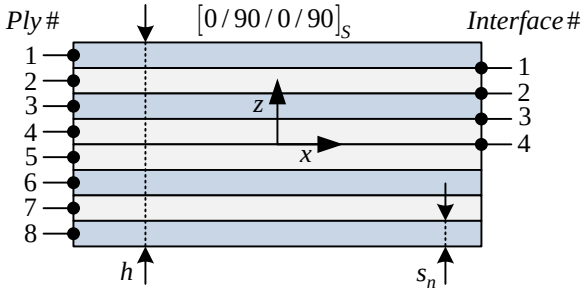

Figure 2. Laminate beam cross-section detail

Table 1. T300/934 Lamina properties[2]

Property	Symbol	Value	Unit
Beam Length	L	127	mm
Beam Width	b	12.7	mm
Beam Thickness	h	1.016	mm
Ply Thickness	s	0.127	mm
Density	ρ	1480	kg/m^3
Poisson's Ratio	$\nu_{12}=\nu_{13}$	0.33	[ ]
Young's Modulus	E_{11}	134.4	GPa
-	$E_{22}=E_{33}$	10.3	GPa
Shear Modulus	$G_{12}=G_{13}$	5.0	GPa
-	G_{23}	3.0 (nominal)	GPa

II. Governing Equations of Motion

In the current study, first order shear deformation theory was used as the governing structural model. Rotation of the transverse normals for a general laminated plate will be defined with the coordinate ψ, and the in-plane displacements of an arbitrary point on the plate can be represented as,

$$u = u^0 + z\psi_x \tag{1}$$

$$v = v^0 + z\psi_y \tag{2}$$

where u^0 and v^0 are the mid-plane displacements of the plate. Upon adding the rotational degree of freedom, the equations of motion can be given as,

$$\frac{\partial N_x}{\partial x} + \frac{\partial N_{xy}}{\partial y} = \rho \frac{\partial^2 u^0}{\partial t^2} \tag{3}$$

$$\frac{\partial N_{xy}}{\partial x} + \frac{\partial N_y}{\partial y} = \rho \frac{\partial^2 v^0}{\partial t^2} \tag{4}$$

$$\frac{\partial M_x}{\partial x} + \frac{\partial M_{xy}}{\partial y} = Q_x + \rho \frac{\partial^2 \psi_x}{\partial t^2} \tag{5}$$

$$\frac{\partial M_{xy}}{\partial x} + \frac{\partial M_y}{\partial y} = Q_y + \rho \frac{\partial^2 \psi_y}{\partial t^2} \tag{6}$$

$$\frac{\partial Q_x}{\partial x} + \frac{\partial Q_y}{\partial y} + N_x^i \frac{\partial^2 w}{\partial x^2} + 2N_{xy}^i \frac{\partial^2 w}{\partial x \partial y} + N_y^i \frac{\partial^2 w}{\partial y^2} + q(x,y) = \rho \frac{\partial^2 w}{\partial t^2} \tag{7}$$

where N and M are the force and moment resultants, q is an applied loading condition, ρ is the beam density, and Q is the shear force. These equations can be derived using Newtonian mechanics or variational principles. For the problem at hand, Eqns. (3)-(7) can be reduced further. First, using constitutive relations derived from classical lamination theory, the force and moment resultants can be written in terms of displacements and rotations. For the symmetric cross-ply beams used in this study, these relations can be given as,

$$\begin{Bmatrix} N_x \\ N_y \\ N_{xy} \\ M_x \\ M_y \\ M_{xy} \end{Bmatrix} = \begin{bmatrix} A_{11} & 0 & 0 & 0 & 0 & 0 \\ 0 & A_{22} & 0 & 0 & 0 & 0 \\ 0 & 0 & A_{66} & 0 & 0 & 0 \\ 0 & 0 & 0 & D_{11} & 0 & 0 \\ 0 & 0 & 0 & 0 & D_{22} & 0 \\ 0 & 0 & 0 & 0 & 0 & D_{66} \end{bmatrix} \begin{Bmatrix} \dfrac{\partial u^0}{\partial x} + \dfrac{1}{2}\left(\dfrac{\partial w}{\partial x}\right)^2 \\ \dfrac{\partial v^0}{\partial y} + \dfrac{1}{2}\left(\dfrac{\partial w}{\partial y}\right)^2 \\ \dfrac{\partial u^0}{\partial y} + \dfrac{\partial v^0}{\partial x} + \dfrac{\partial w}{\partial x}\dfrac{\partial w}{\partial y} \\ -\dfrac{\partial^2 w}{\partial x^2} \\ -\dfrac{\partial^2 w}{\partial y^2} \\ -2\dfrac{\partial^2 w}{\partial x \partial y} \end{Bmatrix} \tag{8}$$

The expressions in Eq. (8) assume $\nu_{xy}=0$ to restrict motion to the *x*-*z* plane. Furthermore, the strain-displacement relations used here retain non-linear terms to allow for buckling analysis if desired. Next, rotations and displacements corresponding to the *y* direction can be ignored to create a two-dimensional problem. The three equations of motion governing the simplified problem are,

$$A_{11}\frac{\partial^2 u^0}{\partial x^2} = \rho A \frac{\partial^2 u^0}{\partial t^2} \tag{9}$$

$$D_{11}\frac{\partial^2 \psi}{\partial x^2} - kA_{55}^*\left(\frac{\partial w}{\partial x} + \psi\right) = \rho I \frac{\partial^2 \psi}{\partial t^2} \tag{10}$$

$$kA_{55}^*\left(\frac{\partial \psi}{\partial x} + \frac{\partial^2 w}{\partial x^2}\right) - P\left(\frac{\partial^2 w}{\partial x^2}\right) = \rho A \frac{\partial^2 w}{\partial t^2} \tag{11}$$

where A is the cross-secitonal area, I is the area moment of inertia, P is the axial load, and κ is the shear correction factor. The stiffness properties of the composite beam in Eqns. (9) - (11) are found using classical lamination theory. Equations (12) - (14) below define the axial, bending, and shear stiffness terms respectively.

$$A_{11} = \int_{-h/2}^{h/2} \bar{Q}_{11} dz = \sum_{k=1}^{n} (\bar{Q}_{11})_k (s_k - s_{k-1}) \tag{12}$$

$$D_{11} = \int_{-h/2}^{h/2} z^2 \bar{Q}_{11} dz = \frac{1}{3}\sum_{k=1}^{n} (\bar{Q}_{11})_k (s_k^3 - s_{k-1}^3) \tag{13}$$

$$A_{55}^* = \int_{-h/2}^{h/2} \bar{C}_{55} dz = \sum_{k=1}^{n} (\bar{C}_{55})_k (s_k - s_{k-1}) \tag{14}$$

The variable h is the total beam thickness, the subscript k denotes the ply layer number, s is the ply thickness, and n is the number of plys. The constants $\bar{C}_{55}$ and $\bar{Q}_{11}$ for each ply depend on the ply stiffness properties and fiber orientation angle. Expressions for these constants can be given as,

$$\begin{aligned} \bar{C}_{55} &= 2\left(G_{23}\sin^2\theta + G_{12}\cos^2\theta\right) \\ \bar{Q}_{11} &= Q_{11}\cos^4(\theta) + Q_{22}\sin^4(\theta) + 2\left(Q_{12} + 2Q_{66}\right)\sin^2\theta\cos^2\theta \end{aligned} \tag{15}$$

where θ is the fiber orientation angle with respect to the *x*-axis, G is the sear modulus, and Q are elements of the inverted compliance matrix for a transversely isotropic material subject to a plain stress loading condition.

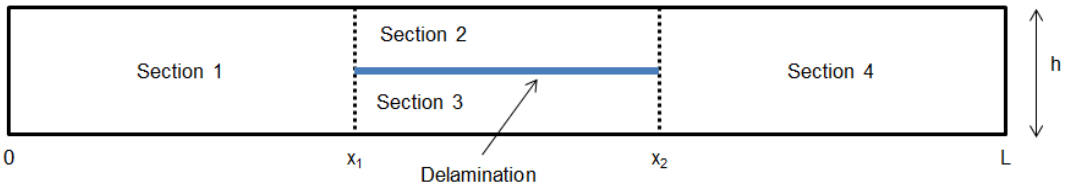

Figure 3. Schematic of simplified delaminated beam using four connected beam sections.

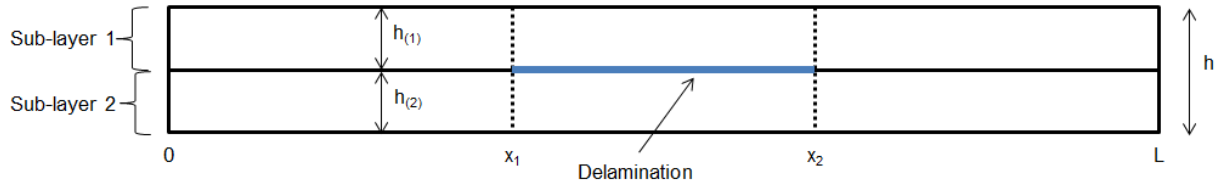

Figure 4. Schematic of simplified delaminated beam using six connected beam sections.

III. Model Development and Theory

Several previous studies have developed methods for modeling delaminations in composite beams. In one such model, presented by Luo and Hanagud[6], the composite beam is divided into four sections. First, the undamaged ends of the beam are modeled as complete beam sections. The middle section of the beam span is divided into two sub-layers, which are separated at the delaminated interface, as shown in Fig 3. Each section of the beam is governed by its own set of equations of motion, yielding four sets of equations of the same form as Eqns. (9) - (11).

Luo and Hanagud explain that partially intact matrix and fibers still exist between the two plies surrounding the delamination[6]. The effect of these materials can be modeled as two distributed soft springs between the delaminated plies. The first spring responds to motion transverse to the beam axis, and its effect can be represented as Eq. (16), where the superscripts (1) and (2) represent the upper and lower sub-layer, respectively, in the delaminated region.

$$\sigma = k_N (w^{(1)} - w^{(2)}) \tag{16}$$

The second distributed spring responds to relative axial displacements between the two sub-layers. This spring represents the friction between the two sub-layers and is often called the linear (or shear) bridging model. The friction stress is is defined in Eq. (17) below.

$$\tau = k_S \left(u^{(1)} - \frac{h_{(1)}}{2} \psi^{(1)} - u^{(2)} - \frac{h_{(2)}}{2} \psi^{(2)} \right) \tag{17}$$

The spring constants k_N and k_S in Eq. (16) and (17) can be adjusted to account for varying degrees of assumed friction between the delaminated surfaces during vibration. Formal definitions for k_N and k_S are provided in Eqns. (18) and (19).

It has been noted since this and similar models were introduced that they contain a major flaw. By treating each intact region as one pristine beam, the rotations of the delaminated sub-layers are constrained to be identical at the ends of the delamination, which produces an artificially stiff model[7]. Qiao and Chen proposed an alternative model, where the composite beam is divided into two complete sub-layers separated at the interface containing the delamination[4]. Furthermore, the beam is divided into three regions along the span of the beam: a pristine region at each end of the beam and a middle section corresponding to the delaminated region. This configuration results in the beam being composed of six distinct sections, as shown in Fig. 4. The delaminate interface is modeled as a distributed spring. Division of the pristine sections into sublayers also requires that the two pristine sections be 'joined' using an interface model. This is accomplished using the same model as in Eq. (16-17), but the spring constants in the pristine sections are dependent on the material properties of the lamina and do not change. The interface stiffness terms can be found using the following expressions.

$$k_N = C_N = \frac{1}{(C_{n1} + C_{n2})} \qquad k_S = C_S = \frac{1}{(C_{s1} + C_{s2})} \tag{18}$$

$$C_{si} = \frac{h_{(i)}}{15G_{13}} \qquad C_{ni} = \frac{h_{(i)}}{10E_{33}} \tag{19}$$

With the beam divided into six sub-sections, 18 coupled differential equations of motion are used to describe the system. The resulting problem is treated as a boundary value problem. Where each of the beam's three spanwise regions yields a sixth order polynomial characteristic equation in terms of a dummy variable where the six solutions of each characteristic equation are complex conjugates. Each of the twelve roots has a corresponding eigenvector of six terms. When all three spanwise regions are considered, there are a total of 36 roots and 36 six-term eigenvectors that must be solved. For a given displacement component, say *u*, in one of the regions, the total displacement field can be represented as the sum of the 12 eigenvectors. This boundary value problem results in 252 unknown terms, 36 of which are independent. Thus, 36 boundary conditions and continuity conditions must be used to completely characterize the dynamic behavior of the beam.

IV. Rayleigh-Ritz Approach

Rather than solving the complex boundary value problem previously described, this work uses a Rayleigh-Ritz approach to determine the dynamic behavior of the subject beams. First, based on Timoshenko beam formulation, the potential and kinetic energy of the beam are defined in Eq. (20) and (21) respectively.

$$\begin{aligned}\Pi_{Total} = \frac{1}{2}\int_0^L \Bigg[& D_{11}^{(1)}\left(\frac{\partial \psi^{(1)}}{\partial x}\right)^2 + kA_{55}^{*(1)}\left(\frac{\partial w^{(1)}}{\partial x} - \psi^{(1)}\right)^2 + A_{11}^{(1)}\left(\frac{\partial u^{(1)}}{\partial x}\right)^2 - P\left(\frac{\partial w^{(1)}}{\partial x}\right)^2 + \ldots \\ & D_{11}^{(2)}\left(\frac{\partial \psi^{(2)}}{\partial x}\right)^2 + kA_{55}^{*(2)}\left(\frac{\partial w^{(2)}}{\partial x} - \psi^{(2)}\right)^2 + A_{11}^{(2)}\left(\frac{\partial u^{(2)}}{\partial x}\right)^2 - P\left(\frac{\partial w^{(2)}}{\partial x}\right)^2 + \ldots \\ & k_N (w^{(1)} - w^{(2)})^2 + k_S\left(u^{(1)} - \frac{h_{(1)}}{2}\psi^{(1)} - u^{(2)} - \frac{h_{(2)}}{2}\psi^{(2)}\right)^2 \Bigg] dx\end{aligned} \tag{20}$$

$$\begin{aligned}T_{Total} = \frac{1}{2}\int_0^L \Bigg[& (\rho A)^{(1)}\left(\frac{\partial u^{(1)}}{\partial t}\right)^2 + (\rho A)^{(1)}\left(\frac{\partial w^{(1)}}{\partial t}\right)^2 + (\rho I)^{(1)}\left(\frac{\partial \psi^{(1)}}{\partial t}\right)^2 + \ldots \\ & (\rho A)^{(2)}\left(\frac{\partial u^{(2)}}{\partial t}\right)^2 + (\rho A)^{(2)}\left(\frac{\partial w^{(2)}}{\partial t}\right)^2 + (\rho I)^{(2)}\left(\frac{\partial \psi^{(2)}}{\partial t}\right)^2 \Bigg] dx\end{aligned} \tag{21}$$

As before, the superscripts (1) and (2) denote upper and lower sub-layers of the beam respectively. Potential energy due to an applied axial load P is included in Eq. (20). Terms associated with the axial load are used to setup and solve the buckling problem as will be seen later. The energy formulation in Eq. (20) and (21) preserves the distributed spring model used in the Qiao/Chen study[7]. Potential energy of the normal and shear spring terms is included in the last line of Eq. (20)

In the proposed model, the beam is separated into two sub-layers that extend the entire beam length. The model therefore contains three degrees of freedom for both sub-layers: axial displacement, transverse displacement and rotation of the transverse normal. Previous works by Zhu[8], Zhou and Cheung[9], and Auciello and Ercolano[10] contain thorough descriptions of the Rayleigh Ritz formulation methods for Timoshenko beams with multiple degrees of freedom. Following a similar procedure, the solution forms for deflections of both sublayers are represented in Eq. (22) as six finite, convergent, summation series functions.

$$
\begin{aligned}
w^{(1)} &= \sum_{i=1}^{N} a_i W_i \qquad & \psi^{(1)} &= \sum_{i=1}^{N} c_i \Psi_i \qquad & u^{(1)} &= \sum_{i=1}^{N} e_i U_i \\
w^{(2)} &= \sum_{i=1}^{N} b_i W_i \qquad & \psi^{(2)} &= \sum_{i=1}^{N} d_i \Psi_i \qquad & u^{(2)} &= \sum_{i=1}^{N} f_i U_i
\end{aligned}
\tag{22}
$$

Coefficients a through f in Eq. (22) are weighting terms associated with their shape functions W, Ψ, and U which correspond to bending, shear, and axial deformations respectively. Notice that there are six degrees of freedom and only three shape function forms. Here it has been assumed that the shape functions associated with each deflection type in sublayer #1 are equal to those in sublayer #2.

After substituting Eq. (22) into Eq. (20) and (21), the mass and stiffness matrices are formed by taking the partial derivatives of the energy expressions with respect to the shape function coefficients a_i, b_i, c_i, d_i, e_i, and f_i. The resulting mass and stiffness matrices have the following partitioned form,

$$
[K] = \begin{bmatrix}
[K_{11}] & [K_{12}] & [K_{13}] & [0] & [0] & [0] \\
 & [K_{22}] & [0] & [K_{24}] & [0] & [0] \\
 & & [K_{33}] & [K_{34}] & [K_{35}] & [K_{36}] \\
 & & & [K_{44}] & [K_{45}] & [K_{46}] \\
 & & & & [K_{55}] & [K_{56}] \\
Sym^T & & & & & [K_{66}]
\end{bmatrix}
\tag{23}
$$

$$
[M] = \begin{bmatrix}
[M_{11}] & & & & & \\
 & [M_{22}] & & & & \\
 & & [M_{33}] & & & \\
 & & & [M_{44}] & & \\
 & & & & [M_{55}] & \\
diag & & & & & [M_{66}]
\end{bmatrix}
\tag{24}
$$

where the individual sub-matrices are calculated without difficulty using the formulas provided in the appendix. Once the mass and stiffness matrices are fully formed, they can be arranged into the typical structural dynamics eigenvalue problem as in Eq. (25).

$$
[K]\begin{Bmatrix} \{a\} \\ \{b\} \\ \{c\} \\ \{d\} \\ \{e\} \\ \{f\} \end{Bmatrix} - \omega^2 [M]\begin{Bmatrix} \{a\} \\ \{b\} \\ \{c\} \\ \{d\} \\ \{e\} \\ \{f\} \end{Bmatrix} = \{0\}
\tag{25}
$$

Solving Eq. (25) yields natural frequencies ω from the eigenvalues, and mode shape weighting terms a through f from the eigenvectors. It is then possible to calculate the Rayleigh-Ritz mode shapes using Eq. (22).

A. Implementation and Choice of Shape Functions for Rayleigh-Ritz Approach

Accuracy of the Rayleigh-Ritz model depends on both the quality of shape functions and the number of terms (N) used to provide the total mode shape expression for each of the six degrees of freedom. The basic requirements for all shape functions are that they must satisfy the geometric boundary conditions of their corresponding degree of freedom and they must be p-times differentiable. The variable p is the order of the highest derivative in the potential

energy expression on the degree of freedom corresponding to the shape function in question. In numeric formulations of structural dynamics problems where shear deformation and rotary inertia are considered, a well-known numerical phenomenon called *shear locking* can occur. Shear locking can cause numeric errors that result in a lack of convergence on a solution and highly inaccurate predictions. In an attempt to avoid these numeric errors, a technique called the Gram-Schmidt iterative procedure presented by Bhat[11] and used in a related study by Auciello and Ercolano[10] was used in the proposed model procedure.

The goal of the Gram-Schmidt procedure is to provide a series of polynomials that are both orthogonal and orthonormal to each other. These are attractive attributes for shape functions used in numerical methods because the likelihood of shear locking is minimal. The procedure begins by selecting an approximate first mode function for each degree of freedom that satisfies the previously stated requirements. The first, second, and *k*th polynomial of each degree of freedom can be expressed as,

$$\begin{aligned} W_0 &= x^{i+1} & W_1 &= (x-A_1)W_0 & W_k &= (x-A_k)W_{k-1} - D_k W_{k-2} \\ \Psi_0 &= x^{i} & \Psi_1 &= (x-B_1)\Psi_0 & \Psi_k &= (x-B_k)\Psi_{k-1} - E_k \Psi_{k-2} \\ U_0 &= x^{i} & U_1 &= (x-C_1)U_0 & U_k &= (x-C_k)U_{k-1} - F_k U_{k-2} \end{aligned} \tag{26}$$

where the shape functions associated with bending W, are an order higher than those for shear Ψ, and axial deformation U. The coefficient expressions from equations (26) are defined as,

$$A_k = \frac{\int_0^\ell x W_{k-1}^2 dx}{\int_0^\ell W_{k-1}^2 dx} \qquad B_k = \frac{\int_0^\ell x \Psi_{k-1}^2 dx}{\int_0^\ell \Psi_{k-1}^2 dx} \qquad C_k = \frac{\int_0^\ell x U_{k-1}^2 dx}{\int_0^\ell U_{k-1}^2 dx}$$

$$D_k = \frac{\int_0^\ell x W_{k-1} W_{k-2} dx}{\int_0^\ell W_{k-2}^2 dx} \qquad E_k = \frac{\int_0^\ell x \Psi_{k-1} \Psi_{k-2} dx}{\int_0^\ell \Psi_{k-2}^2 dx} \qquad F_k = \frac{\int_0^\ell x U_{k-1} U_{k-2} dx}{\int_0^\ell U_{k-2}^2 dx} \tag{27}$$

Where all of the polynomials generated are forced to be orthonormal functions which satisfy the following condition.

$$\int_0^\ell \phi_k(x)\phi_l(x)dx = \begin{Bmatrix} 0 & if \quad k \neq l \\ 1 & if \quad k = l \end{Bmatrix} \tag{28}$$

Generating these polynomials can be accomplished with most readily available numeric programming software packages. In this work the authors used MATLAB™ to write a simple function capable of generating hundreds of these polynomials along with their derivatives where the computational effort was only a small fraction of the entire code.

B. Damage Modeling with the Rayleigh-Ritz Method

Delamination was simulated by modifying the interfacial shear and normal stiffness terms defined in Eq. (18) and (19). In order to localize the damage, it is convenient to define the interface conditions as piecewise continuous functions of x. From the definition of the stiffness terms for Eq. (23) (shown in the appendix) it is clear that the effects of defining interface conditions as functions of *x* are accounted for by integrating over the entire beam length. Therefore, a local decrease in stiffness contributes to an overall decrease in the submatrix associated with the specified damage type. The interface stiffness functions can be defined as,

$$\begin{aligned} k_N(x) &= k_N\left[H(x_1-x) + d_N H(x-x_1)H(x_2-x) + H(x-x_2)\right] \\ k_S(x) &= k_S\left[H(x_1-x) + d_S H(x-x_1)H(x_2-x) + H(x-x_2)\right] \end{aligned} \tag{29}$$

where k_N and k_S are pristine stiffness values from Eq. (18) and (19), d_N and d_S are normal and shear damage metrics respectively, x_1 and x_2 are *x*-coordinates corresponding to the damage boundaries as shown in Fig. 4, and H is the Heaviside step function defined as,

$$H(x) = \begin{Bmatrix} 0 & for & x < 0 \\ 1 & for & x > 0 \end{Bmatrix} \tag{30}$$

For the case of total delamination in the region between x_1 and x_2 both damage metrics were set to zero. Partial delamination and the effect of friction in the delaminated region could be investigated simply by setting d_N and d_S to some reduced percentage of their pristine value.

C. Modification of Rayleigh-Ritz Procedure to Predict Buckling Behavior

The axial load *P* in the equations of motion will cause an increase in natural frequency when the beam is in tension and will decrease the natural frequency when in compression. The lowest load that drives the natural frequency to zero will be the critical buckling load. The general structural eigenvalue problem first given in Eq. (25) can be expressed as,

$$\left([\mathbf{K}_v] - P[\mathbf{K}_b] - \omega^2 [\mathbf{M}] \right) \{\mathbf{q}\} = 0 \tag{31}$$

where $\mathbf{K}_b$ is a matrix that contains only stiffness terms that are coefficients of the axial load which are taken directly from the original stiffness matrix $\mathbf{K}$. It is then straightforward to define $\mathbf{K}_v$ as a matrix containing all remaining stiffness elements i.e. all elements of the original stiffness matrix that do not contain axial load terms. A new eigenvalue problem is formed when $\omega \to 0$,

$$\left([\mathbf{K}_v] - P[\mathbf{K}_b] \right) \{\mathbf{q}\} = 0 \tag{32}$$

where the eigenvalues of this system are in fact 'eigenloads' P_i such that the lowest eigenvalue corresponds to the critical buckling load of the system P_{cr}. Solutions are found by setting the determinant of $(\mathbf{K}_v - P\mathbf{K}_b)$ equal to zero and solving for P.

V. Finite Element Modeling

A finite element model was constructed using the PAM-CRASH software program from the ESI Group. Each composite ply was modeled as a series of shell elements with material properties adjusted for the ply orientation. A schematic of the model is shown in Fig. 5.

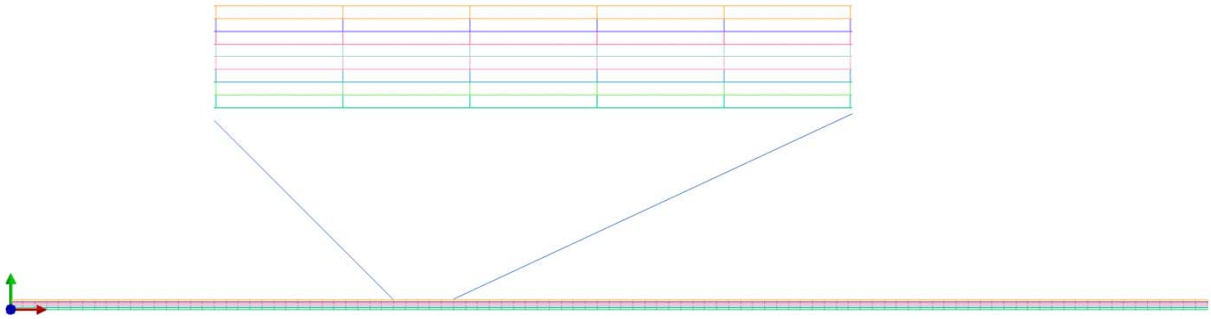

Figure 5. Finite element model configuration

To allow for delaminated interfaces in the model, each ply was modeled as a distinct set of shell elements with its own set of nodes. Intact portions of each interface were then modeled using the LINK/TIED option within the software. For areas of each ply interface intended to represent a delamination, the adjacent elements were not linked in this manner. Calculation of the structural vibration behavior of the beam was done using the EIGEN control option within the PAM-CRASH software.

VI. Results and Comparisons

Preliminary numerical studies were performed with the Rayleigh-Ritz model to explore the effects of various delamination length and locations on fundamental frequency, buckling loads, and mode shapes. The following is a summary and brief discussion of initial results from the proposed analytical and FEM models.

A. Effect of Delamination Length

The results shown here are for the case where various delaminations occurred at interface #4 and were centered about the midspan. Figure 6 shows the finite element model mode shapes and Fig. 7 shows the Rayleigh-Ritz mode shapes attained using the proposed model. These mode shapes are calculated using 40%, 60%, and 80% delamination lengths and are compared to the mode shape of a pristine beam. All mode shapes were normalized to produce a tip deflection of one unit. As the figures show, the proposed model successfully captured the mode shape changes due to the midspan delaminations.

It can be seen in Fig. 8 that at higher damage lengths the proposed Rayleigh-Ritz model is able to closely predict the correct natural frequency trend from experimental results presented in the recent study by Qiao and Chen[7]. As one would expect, Rayleigh-Ritz overestimates the fundamental frequency observed in experiments.

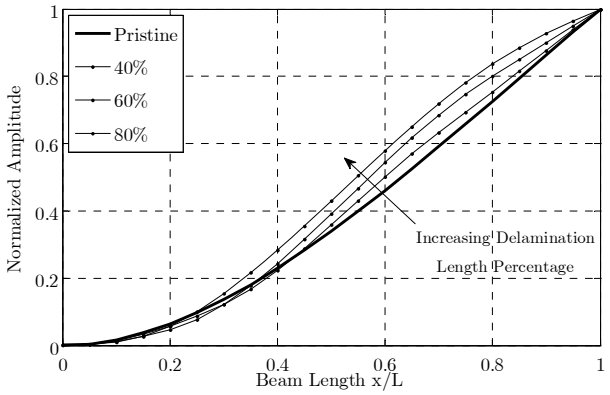

Figure 6. FEM results showing the effect of delamination length on fundamental vibration mode shape for interface #4.

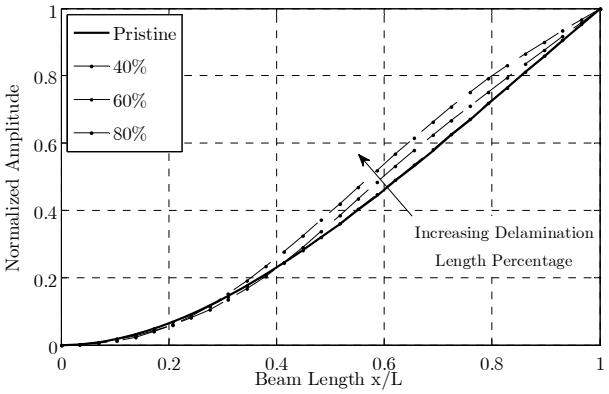

Figure 7. Rayleigh-Ritz model results showing the effect of delamination length on fundamental vibration mode shape for interface #4.

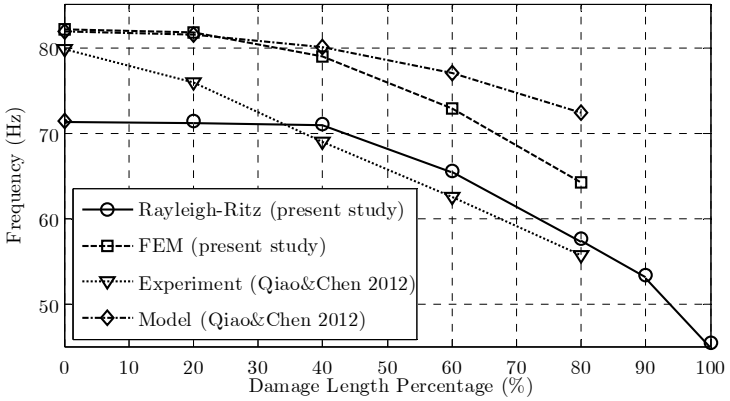

Figure 8. Effect of delamination length on fundamental vibration frequency with comparisons to finite element model and results from literature.

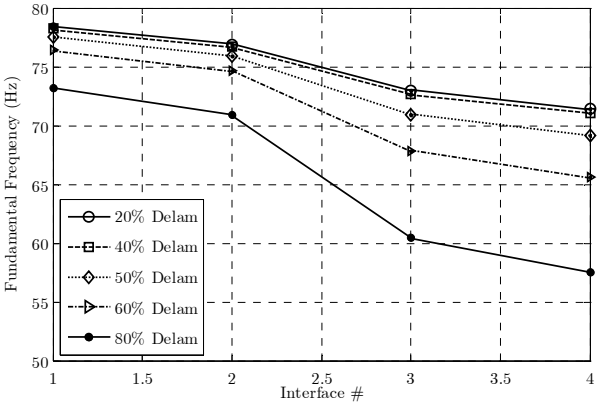

Figure 9. Effect of a given delamination at various laminate interface levels on fundamental vibration frequency

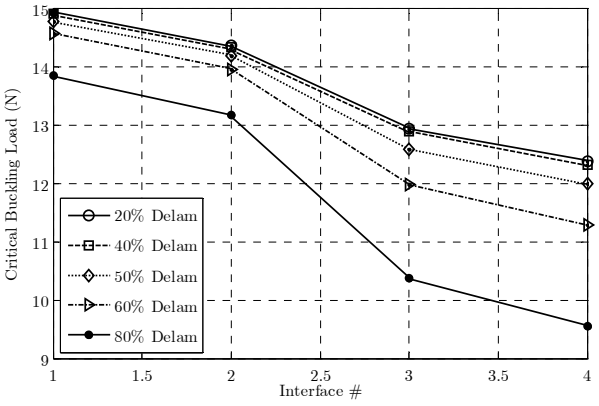

Figure 10. Effect of a given delamination at various laminate interface levels on critical buckling load

B. Effect of Delamination Interface

Figures 9 and 10 show trends in natural frequency and critical buckling load for a given damage length percentage as a function of the interface number at which the delamination occurs. Interface #1 corresponds to the interface between layers #1 and #2, i.e. the interface furthest from the neutral axis (see Fig. 2). The results in figures 9 and 10 show that as a delamination occurs closer to the neutral axis both fundamental frequency and critical buckling load decrease significantly.

VII. Conclusions

Modeling delamination effects in beams with bending, first-order shear, and axial deformation using a six degree-of-freedom Rayleigh-Ritz approach proved to be extremely convenient compared to other popular approaches used in the literature. Material properties and interface conditions that varied along the beam length could easily be accounted for. Upon using the Rayleigh-Ritz approach, it is clear how one could expand the model presented in this work to account for more complex structures with various boundary conditions. Features such as distributed loads, point masses, and geometric properties that vary along beam length could all be implemented using techniques shown in this paper.

From the results, one can see how various delaminations reduce natural frequencies, reduce critical buckling loads and modify mode shapes. An expected yet interesting result represented by the model was that as delamination length increased and ultimately created two separate beams, the first two natural frequencies and first two critical buckling loads approached exact analytical values one would find using properties of each sublayer. It was also observed that the natural frequency was most sensitive to a delamination located at the beam root between the two center plys (center thickness).

Acknowledgments

The authors would like to thank Dr. Anthony Waas for being the primary research advisor for this project, and Dr. Wooseok Ji for his assistance in constructing the finite element model used for this work. The authors also gratefully acknowledge the financial support of the University of Michigan College of Engineering.

Appendix

A. Equations for Rayleigh-Ritz Mass Sub-matrices used in Eq. 24

$$[M_{11}] = \int_0^L m^{(1)} W_i W_j dx \qquad [M_{44}] = \int_0^L (\rho I)^{(2)} \Psi_i \Psi_j dx$$

$$[M_{22}] = \int_0^L m^{(2)} W_i W_j dx \qquad [M_{55}] = \int_0^L m^{(1)} U_i U_j dx$$

$$[M_{33}] = \int_0^L (\rho I)^{(1)} \Psi_i \Psi_j dx \qquad [M_{66}] = \int_0^L m^{(2)} U_i U_j dx$$

B. Equations for Rayleigh-Ritz Stiffness Sub-matrices used in Eq. 23

$$[K_{11}] = \int_0^L \left[\left(\kappa A_{55}^{*(1)} - P \right) \frac{\partial W_i}{\partial x} \frac{\partial W_j}{\partial x} + k_N W_i W_j \right] dx$$

$$[K_{12}] = -\int_0^L k_N W_i W_j dx$$

$$[K_{22}] = \int_0^L \left[\left(\kappa A_{55}^{*(2)} - P \right) \frac{\partial W_i}{\partial x} \frac{\partial W_j}{\partial x} + k_N W_i W_j \right] dx$$

$$[K_{13}] = -\int_0^L \kappa A_{55}^{*(1)} \Psi_i \frac{\partial W_i}{\partial x} dx$$

$$[K_{24}] = -\int_0^L \kappa A_{55}^{*(2)} \Psi_i \frac{\partial W_i}{\partial x} dx$$

$$[K_{33}] = \int_0^L \left[D_{11}^{(1)} \frac{\partial \Psi_i}{\partial x} \frac{\partial \Psi_j}{\partial x} + \kappa A_{55}^{*(1)} \Psi_i \Psi_j + \frac{h_{(1)}^2}{4} k_S \Psi_i \Psi_j \right] dx$$

$$[K_{34}] = \int_0^L \frac{h_{(1)} h_{(2)}}{4} k_S \Psi_i \Psi_j dx$$

$$[K_{44}] = \int_0^L \left[D_{11}^{(2)} \frac{\partial \Psi_i}{\partial x} \frac{\partial \Psi_j}{\partial x} + \kappa A_{55}^{*(2)} \Psi_i \Psi_j + \frac{h_{(2)}^2}{4} k_S \Psi_i \Psi_j \right] dx$$

$$[K_{35}] = -\int_0^L \frac{h_{(1)}}{2} k_S \Psi_i U_i dx$$

$$[K_{36}] = \int_0^L \frac{h_{(1)}}{2} k_S \Psi_i U_i dx$$

$$[K_{45}] = -\int_0^L \frac{h_{(2)}}{2} k_S \Psi_i U_i dx$$

$$[K_{46}] = \int_0^L \frac{h_{(2)}}{2} k_S \Psi_i U_i dx$$

$$[K_{55}] = \int_0^L \left[A_{11}^{(1)} \frac{\partial U_i}{\partial x} \frac{\partial U_j}{\partial x} + k_S U_i U_j \right] dx$$

$$[K_{56}] = -\int_0^L k_S U_i U_j dx$$

$$[K_{66}] = \int_0^L \left[A_{11}^{(2)} \frac{\partial U_i}{\partial x} \frac{\partial U_j}{\partial x} + k_S U_i U_j \right] dx$$

References

[1]Della, C. N., and Shu, D. Vibration of Delaminated Composite Laminates: A Review, *Applied Mechanics Reviews*, 2007, Vol. 60.

[2]Ramkumar, R. L., Kulkarni, S. V., and Pipes, R. B. Free Vibration Frequencies of a Delaminated Beam, *34th Annual Technical Conference Proceedings, Reinforced/Composite Institute, Society of Plastics Industry*. Sec 22-E, pp . 1-5.

[3]Mujumdar, P., and Suryanarayan, S., Flexural vibrations of beams with delaminations, *Journal of sound and vibration*, 1988, Vol. **125**, pp. 441–461.

[4]Shen, M. H. H., and Grady, J., Free vibrations of delaminated beams, *AIAA journal*, 1992, Vol. **30**, pp. 1361–1370.

[5]Della, C. N., and Shu, D., Free vibration analysis of composite beams with overlapping delaminations, *European Journal of Mechanics-A/Solids*, 2005, Vol. **24**, pp. 491–503.

[6]Luo, H., and Hanagud, S., Dynamics of delaminated beams, *International journal of solids and structures*, 2000, Vol. **37**, pp. 1501–1519.

[7]Qiao, P., and Chen, F., On the improved dynamic analysis of delaminated beams, *Journal of Sound Vibration*, 2012, Vol. **331**, pp. 1143–1163.

[8]Zhu, T. L., The vibrations of pre-twisted rotating Timoshenko beams by the Rayleigh-Ritz method, *Computational Mechanics*, 2011, Vol. **47**, pp. 395–408.

[9]Zhou, D., and Cheung, Y., Vibrations of tapered Timoshenko beams in terms of static Timoshenko beam functions, *Journal of applied mechanics*, 2001, pp. Vol. **68**, 596.

[10]Auciello, N., and Ercolano, A., A general solution for dynamic response of axially loaded non-uniform Timoshenko beams, *International journal of solids and structures*, 2004, Vol. **41**, pp. 4861–4874.

[11]Bhat, R., Natural frequencies of rectangular plates using characteristic orthogonal polynomials in Rayleigh-Ritz method, *Journal of Sound and Vibration*, 1985, Vol. **102**, pp. 493–499.